# Mechanosensitive shivering of model tissues under controlled aspiration

Karine Guevorkian[a,1,2], David Gonzalez-Rodriguez[a,2], Camille Carlier[b], Sylvie Dufour[b], and Françoise Brochard-Wyart[a,1]

[a]Institut Curie, Centre National de la Recherche Scientifique, Unité Mixte de Recherche 168, and University Paris 6, 75248 Paris Cedex, France; and [b]Institut Curie, Centre National de la Recherche Scientifique, Unité Mixte de Recherche 144, 75248 Paris Cedex, France

Edited by David A. Weitz, Harvard University, Cambridge, MA, and approved June 14, 2011 (received for review April 20, 2011)

**During embryonic development and wound healing, the mechanical signals transmitted from cells to their neighbors induce tissue rearrangement and directional movements. It has been observed that forces exerted between cells in a developing tissue under stress are not always monotonically varying, but they can be pulsatile. Here we investigate the response of model tissues to controlled external stresses. Spherical cellular aggregates are subjected to one-dimensional stretching forces using micropipette aspiration. At large enough pressures, the aggregate flows smoothly inside the pipette. However, in a narrow range of moderate aspiration pressures, the aggregate responds by pulsed contractions or "shivering." We explain the emergence of this shivering behavior by means of a simple analytical model where the uniaxially stretched cells are represented by a string of Kelvin–Voigt elements. Beyond a deformation threshold, cells contract and pull on neighboring cells after a time delay for cell response. Such an active behavior has previously been found to cause tissue pulsation during dorsal closure of *Drosophila* embryo.**

cell pulsation | tissue viscoelasticity | biological oscillations | multicellular dynamics | myosin contractility

Tissue rearrangement and movement during development require cells to respond to mechanical cues of their environment and transmit signals to their neighbors. For example, tissue deformation or compression can stimulate the expression of patterning genes (1) and induce Myosin II apical redistribution to produce cell constriction (2). Cells respond to mechanical signals by changing their shape, motility, and contractility. For instance, environmental stiffness affects cell spreading, proliferation, survival, and migration properties and dictates stem cell fate (3). Mechanosensitivity and mechanotransduction take place between cells and at the cell-matrix contact site, and they require the actomyosin network (4, 5). Cadherins and integrins are adhesion receptors controlling intercellular adhesion and interactions with extracellular matrices, respectively. They act as mechanoreceptors linking external ligands with the cell cortex and cytoskeleton (6–8). Forces generated through the cortical tension induce cell shape changes and result in directional movement of the tissue (9), tissue segregation (10), and cellular pulsation (11).

Coordinated cellular contractions in the form of apical constrictions play a key role in morphogenesis (12), such as in sea urchin gastrulation (13) or neural tube closure (14). In some such systems, coordinated pulsatile cell contractions have been proposed to drive morphogenetic movements, such as in *Drosophila* gastrulation (11) and dorsal closure (15). Recently, Solon et al. (15) have described the mechanism of cellular pulsation of amnioserosa cells during the dorsal closure of *Drosophila* embryo. Notably, the observed pulsatile behavior does not require individual cells to actively oscillate. Instead, the active response of a single cell is a delayed contractile force that depends only on the cell's earlier degree of stretching, and the collective pulsatile behavior arises from cellular interactions. Solon et al. developed a numerical model to explain the emergence of this behavior in the relatively complex two-dimensional amnioserosa tissue of relevance in *Drosophila* (15). Here we investigate the response of cellular aggregates to a one-dimensional aspiration force, a simpler configuration where a resembling pulsatile phenomenon arises.

Spherical cellular aggregates are widely used as in vitro model systems to study the mechanical properties of tissues. It has been shown that cellular aggregates behave like viscoelastic liquids possessing a surface tension (16). The mechanical properties of cellular aggregates have been characterized by parallel-plate compression (16, 17), micropipette aspiration (18), and aggregate centrifugation (19). The origin of the surface tension has not been fully elucidated, but the cellular cortical tension (which determines the surface tension of a single cell) and the cell–cell adhesion have been identified as the two major responsible mechanisms (20–22). Guevorkian et al. previously described the micropipette aspiration of E-cadherin-expressing cell aggregates, which they modeled using an analogy with a viscoelastic fluid with a surface tension (18). They found that, unlike an inert fluid, the surface tension of a cell aggregate increases with the applied aspiration pressure (18). This increase in the effective surface tension was interpreted as an active response of cells to the external stress. In this study, we explore a mechanosensitive cell response observed in a narrow range of pressures and for aggregates of small size. In such confined range of pressures, we observe that aggregates do not flow monotonically inside the pipette as previously described, but they exhibit pulsed contractions that we call shivering. This shivering behavior can be explained by introducing an active cell response into the previous viscoelastic model. A certain time after a cell is stretched beyond a threshold, the cell exerts a contractile force on neighboring cells. If the external aspiration pressure is such that the resulting cell stretching remains close to the threshold, cells switch on and off their active contraction, which results in shivering.

## Results

Fig. 1*A* shows a schematic of our experimental setup. An aggregate of radius $R_0$ is aspirated inside a pipette of radius $R_p$ at a constant pressure $\Delta P$. Considering that the aggregate possesses a surface tension $\gamma$, the aspiration force is $f = \pi R_p^2(\Delta P - \Delta P_{\min})$, where $\Delta P_{\min}$ is the minimum pressure required for aspiration given by the Laplace equation, $\Delta P_{\min} = 2\gamma(1/R_p - 1/R_0)$. The experiments reported here were performed on aggregates of murine sarcoma cell lines (S180) that express E-cadherin molecules. The response to aspiration is characterized by tracking the instantaneous length of the aggregate tongue aspirated inside the micropipette, denoted by $L(t)$. The micropipette is internally coated with polyethylene glycol-polylysine, so that the aggregate

Author contributions: K.G., D.G.-R., S.D., and F.B.-W. designed research; K.G. and C.C. performed research; S.D. contributed new reagents/analytic tools; K.G. and D.G.-R. analyzed data; and K.G., D.G.-R., S.D., and F.B.-W. wrote the paper.

The authors declare no conflict of interest.

This article is a PNAS Direct Submission.

[1]To whom correspondence may be addressed. E-mail: karine.guevorkian@curie.fr or brochard@curie.fr.

[2]K.G. and D.G.-R. contributed equally to this work.

This article contains supporting information online at www.pnas.org/lookup/suppl/doi:10.1073/pnas.1105741108/-/DCSupplemental.

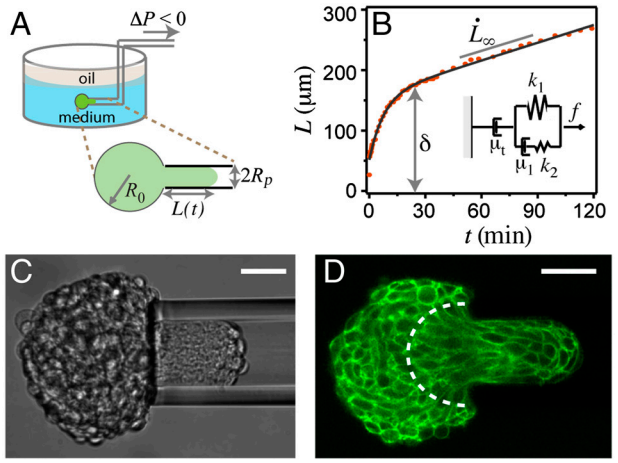


**Fig. 1.** Aspiration of cellular aggregates. (*A*) A schematic of the experimental setup. (*B*) Aspiration curve for an aggregate of the radius $R_0 = 150$ μm and pipette radius $R_p = 38$ μm at $\Delta P = 1{,}300$ Pa. Inset shows the modified Maxwell model used to fit the data. (*C*) Aggregate under aspiration at $\Delta P = 500$ Pa. (Scale bar: 50 μm.) (*D*) Aspirated aggregate observed in confocal microscopy, the cells are transfected with GFP-tagged E-cadherin molecules. The stretched cells are seen inside the pipette and in the deformation zone within a radius $R_p$ into the aggregate body (white dashed line). $\Delta P = 500$ Pa. (Scale bar: 50 μm.)

tongue slips inside the micropipette and the dominant viscous resistance to flow is localized at the micropipette entry. The viscous dissipation zone inside the aggregate is restricted to a distance equal to the radius of the pipette, corresponding to the region of cell deformation shown in Fig. 1*D* (Movie S1). A typical aspiration curve for the case where 1,000 Pa $< \Delta P <$ 2,000 Pa and $R_0/R_p \geq 3$ is shown in Fig. 1*B*. Two regimes can be identified on such a curve: a short-term deformation and a long-term constant flow. By analogy with a viscoelastic liquid, we characterize the aggregate's mechanical behavior using a modified Maxwell model consisting of two springs of constants $k_1$ and $k_2$ and two dampers of impedances $\mu_1$ and $\mu_t$, arranged as shown in the inset of Fig. 1*B* (18). The instantaneous tongue length $L(t)$ is given by $L(t) = (f/k_1)\{1 - [k_2/(k_1 + k_2)]e^{-t/\tau_c}\} + (f/\mu_t)t$. The first term characterizes the short-term, elastic regime with $\tau_c = \mu_1(k_1 + k_2)/(k_1 k_2)$ being the cell viscoelastic time, or the raising time of the elastic deformation $\delta$. The second term characterizes the viscous flow at constant velocity $\dot{L}_\infty = f/\mu_t$. The mechanical parameters can be expressed in terms of the elastic modulus $E$, the cell viscosity $\eta_c$, and the tissue viscosity $\eta_t$ as $k_1 = \pi R_p E$, $\mu_1 = \pi\eta_c R_p$, and $\mu_t = 3\pi^2\eta_t R_p$. The tissue relaxation time separating the elastic and viscous regimes is given by $\tau_t = \mu_t/k_1 = 3\pi\eta_t/E$. Typical values for $\tau_c$ are of the order of 1–5 min, whereas $\tau_t$ is about 45 min. For S180 cellular aggregates, Guevorkian et al. found $E \approx 700$ Pa and $\eta_t \approx 2 \times 10^5$ Pa · s (18).

In this paper we report our findings for the case where the aggregates are subjected to aspiration pressures in the range of 500–1,200 Pa at 37 °C. Note that $\Delta P_{\min}$ is around 200–300 Pa for the cell line and aggregate sizes used here, which corresponds to a resting surface tension of $\gamma_0 \approx 5$ mN/m, as discussed by Guevorkian et al. (18). Unlike the previously described smooth advancement of the aggregate inside the pipette, in an intermediate range of pressures, we observe aggregate contractions. These contractions can be seen in the kymograph of Fig. 2 *A* and *B*. Contractions in the aspirated tongue are sometimes correlated with contractions of the extrenal aggregate body (yellow arrows in Fig. 2*B*) and sometimes uncorrelated (green arrow in Fig. 2*B*) (Movie S2). We could identify two types of contractions. Large contractions have a typical amplitude larger than 3 μm and involve a significant portion of the aggregate. As shown in the kymograph of Fig. 2 *A* and *B*, the contractions of neighboring

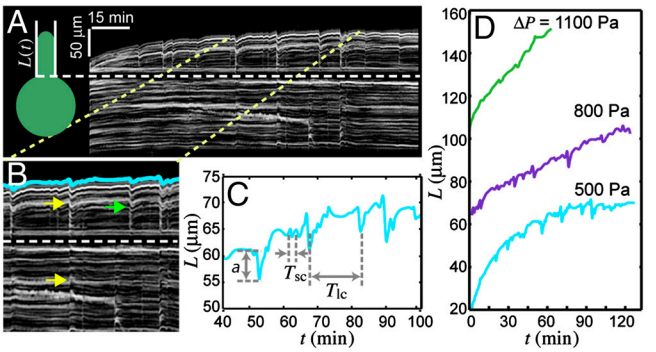


**Fig. 2.** Shivering of a cellular aggregate under aspiration. (*A* and *B*) Kymograph showing the advancement $L(t)$ of the aggregate inside the pipette as a function of time, for an aggregate of $R_0 = 70$ μm and $R_p = 37$ μm, at a pressure of $\Delta P = 500$ Pa (Movie S2). (*C*) Tracking of the leading edge of *B*. Amplitude of the large contractions is represented by *a*, and $T_{sc}$ and $T_{lc}$ are the periods of the small and large contractions, respectively. (*D*) Contractions of the same aggregate when the aspiration pressure is increased in steps.

groups of cells are in phase. Small contractions have a typical amplitude of about 1 μm or less and are typically more localized at random parts of the aggregate (Movie S2). As discussed below, small contractions are interpreted as single-cell responses, whereas large contractions correspond to the synchronized response of several cells. To quantify these pulsations, we developed an edge detection algorithm that determines the position of the front of the aggregate tongue aspirated into the pipette, shown in Fig. 2*B*. We have analyzed the contraction amplitudes, duration of the contractions, and periods between contractions for several experiments, presented in Fig. 2*C*. As an example, we show in Fig. 2*D* the aspiration curves for an aggregate subjected to a stepwise increase of applied pressure, starting at 500 Pa. When the pressure is set to 1,100 Pa, both the number and the amplitude of the contractions diminish.

To characterize the dependence of the large contraction amplitude, $a$, to the applied pressure, for each experiment we have taken the mean value of the five largest amplitudes (or the average of all contractions if there were less than five). As shown in Fig. 3*A*, the amplitude of the contraction decreases as the applied pressure increases. For pressures larger than 1,200 Pa, the amplitudes of the contractions were smaller than the minimum measurable, and in many cases no contraction was observed. For $\Delta P \leq \Delta P_{\min}$, the aggregate does not penetrate inside the pipette, and no contraction is detectable. When $\Delta P$ is slightly above $\Delta P_{\min}$, the aspiration dynamics is very slow and difficult to characterize experimentally. Experimentally quantifiable oscillations appear only at about $\Delta P \approx 500$ Pa. The distribution of amplitudes from several experiments at $\Delta P = 500$ Pa is presented in the inset of Fig. 3*A*. The period of the small contractions, shown as $T_{sc}$ in Fig. 2*C*, is of the order of 200 s as shown in the histogram of Fig. 3*B*. The period between consecutive large contractions varies between 500 s $< T_{lc} <$ 1,000 s. We have also observed that, as the ratio between aggregate and pipette radii becomes larger ($R_0 \geq 3R_p \approx 150$ μm), the large contractions become less frequent and their amplitude decreases, while small contractions remain present regardless of the aggregate size.

## Analysis

We have developed a one-dimensional mechanical model to rationalize the contractions observed during aspiration. As sketched in Fig. 4, the aspirated tongue is idealized as parallel strings of individual cells. The model cell string includes not only cells in the aspirated tongue, but also cells inside the aggregate body that are stretched due to the aspiration, which is felt a distance $R_p$ into the aggregate body outside the pipette. Analogous

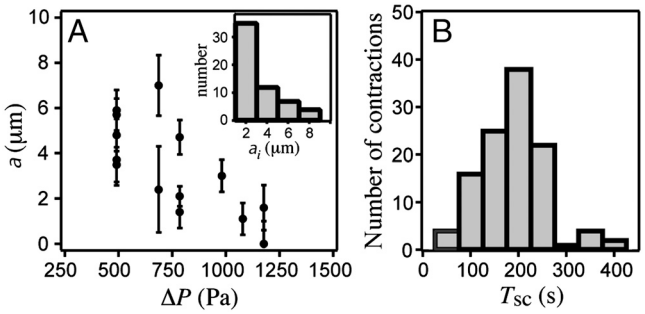


**Fig. 3.** Characterization of aggregate contractions. (*A*) Decrease of the amplitude of the large contractions, *a*, as the stress is increased, error bars are standard deviation. The inset shows the histogram of the contraction amplitudes, $a_i$, observed over five trials at $\Delta P = 500$ Pa. (*B*) Histogram of contraction period for all the aggregates.

to the previous model of the aspiration dynamics (18) summarized above, a viscoelastic cell response to stress is assumed. In this previous model, a Maxwell element represents the response of the whole aspirated tongue. In the model proposed in this article, we use a Kelvin–Voigt element to represent each single cell in the idealized cell string. Such a Kelvin–Voigt element consists of a spring of constant $k_c = (R_c/R_p)k_1 = \pi E R_c$ and a damper of impedance $\mu_c = (R_c/R_p)\mu_1 = \pi\eta_c R_c$, where $2R_c \approx 15$ μm is the undeformed cell diameter. Moreover, we do not account for an instantaneous cell deformation, which amounts to assume $k_2 \gg k_1$ in the previous model. The characteristic time of viscoelastic deformation of a single cell is the cell viscoelastic time, $\tau_c \equiv \eta_c/E \approx 100$ s (18). An external force of magnitude $F_p$, arising from the applied pressure difference, is exerted on the right end. Because our model considers one string of cells and not the complete tongue, this force is given by $F_p = (R_c^2/R_p^2)f = \pi R_c^2(\Delta P - \Delta P_{\min})$. We apply a fixed boundary condition on the left end to reflect that, by continuity, cell motion in the aggregate core is much slower than in the aspirated tongue.

In order to reproduce the observed shivering, it is also necessary to account for the active response of the cells to an applied stress. We use an active response model similar to the one proposed by Solon et al. to describe the cooperative cell oscillations observed during dorsal closure in *Drosophila* (15). Cells are assumed to exert a contractile force of magnitude $F_m$ when they are stretched beyond a critical strain $\epsilon_{\text{crit}}$, whereas the contractile force is zero below this stretching threshold. Such an active contractile response as a response to stretching is consistent with experimental findings for individual cells (23). Mathematically, such a response is represented by a Heaviside step function,

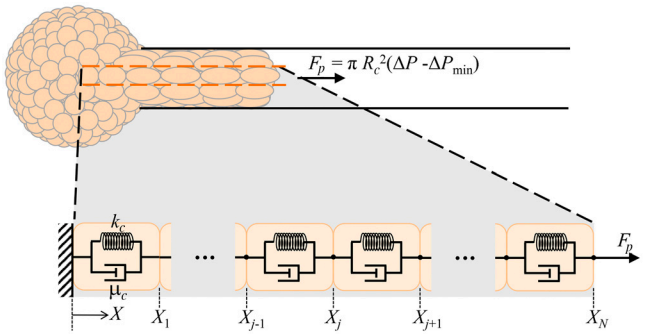


**Fig. 4.** One-dimensional model of aggregate shivering. Each cell is represented as a Kelvin–Voigt element to model the viscoelastic response of the cell. The viscous flow of the tissue is modeled by periodically adding one cell to the left end of the string.

$$F_s(t) = \begin{cases} 0 & \text{if } \epsilon(t-\tau_s) \le \epsilon_{\text{crit}} \\ F_m & \text{if } \epsilon(t-\tau_s) > \epsilon_{\text{crit}}, \end{cases} \quad [1]$$

where $\epsilon$ is the cell strain, and $F_s(t)$ is the contractile force that a cell exerts at time $t$ when it has been strained by $\epsilon$ at time $(t-\tau_s)$. As reflected by Eq. **1**, the contractile force is assumed not to develop immediately upon stretch, but rather after a time delay $\tau_s$.

The system's dynamics is determined by the balance between the viscoelastic and active contractile cell response and the applied aspiration pressure. For a discrete number of cells, $N$, the cell's equation of motion is presented in *Materials and Methods* (Eq. **6**). For large enough $N$, the equation can be written in continuous form as

$$\tau_c \frac{\partial \epsilon}{\partial t} + \epsilon = \frac{F_p - F_s}{2k_c R_c}. \quad [2]$$

This equation is readily integrated to characterize oscillations of the cell strain, $\epsilon$, around the contraction threshold $\epsilon = \epsilon_{\text{crit}}$. For an applied pressure of magnitude $F_p = F_{\text{crit}} + \alpha F_m$, where $F_{\text{crit}} = 2k_c R_c \epsilon_{\text{crit}}$ is the critical pressure force corresponding to the shivering threshold, the resulting period and amplitude of oscillation, $T_{\text{sc}}$ and $\Delta\epsilon$, are

$$e^{T_{\text{sc}}/\tau_c} = 1 + \frac{e^{\tau_s/\tau_c}(e^{\tau_s/\tau_c} - 1)}{\alpha(1-\alpha)} \quad [3]$$

$$\Delta\epsilon = \frac{F_m}{2k_c R_c}(1 - e^{-\tau_s/\tau_c}). \quad [4]$$

Eq. **3** requires that $0 < \alpha < 1$ for oscillations to occur or, equivalently, $F_{\text{crit}} < F_p < F_{\text{crit}} + F_m$. Thus, for oscillations to occur, cells must alternately switch on and off their active contraction, which requires that $F_p > F_{\text{crit}}$ (cells contract under the applied pressure force) and $F_p - F_m < F_{\text{crit}}$ (the contractile force reduces the cell deformation below the contractility threshold). Experimentally we observe that cells contract in the range of pressure of $\Delta P - \Delta P_{\min} \approx 200$–$900$ Pa, from which we deduce that $\epsilon_{\text{crit}} \approx 0.3$ and $F_m \approx 0.1$ μN. For the cell's shivering amplitude to be of the order of 1 μm, as observed experimentally, Eq. **4** implies that $\tau_s/\tau_c \approx 1/5$, which yields a contractile response time of $\tau_s \approx 40$ s, consistent with the value of 100 s reported by Solon et al. (15), and an oscillation period of $T_{\text{sc}} \approx 150$ s, consistent with the experimental observations. Because $\tau_s/\tau_c \ll 1$, Eqs. **3** and **4** can be approximated by $T_{\text{sc}} \approx \tau_s/[\alpha(1-\alpha)]$ and $\Delta\epsilon \approx [F_m/(2k_c R_c)](\tau_s/\tau_c)$.

For a discrete number of cells, $N$, the model can be readily implemented numerically, as detailed in *Materials and Methods*. The simplest model considers a fixed number of cells inside the pipette, $N$, which is an accurate representation of the dynamics at a timescale smaller than the tissue viscoelastic timescale, $\tau_t \approx 45$ min (18). Fig. 5 shows the results of the model for parameter values corresponding to typical experimental conditions. Fig. 5*A*, obtained by running the model with a fixed number of cells, shows the position of the right-most cell edge (black curve) and of all the other cell edges along the one-dimensional cell string (gray curves). Because all cells are assumed identical and the force is applied to all of them at the same time, this simple model predicts oscillations that are in phase along the aspirated tongue. As deduced analytically, the period of oscillation $T_{\text{sc}}$ observed in the figure is related to the active response delay by $T_{\text{sc}} \approx 4\tau_s$. At a timescale comparable to $\tau_t$, the slow flow of cells into the pipette must be considered. This flow can be modeled by introducing one additional cell at the fixed end with a periodicity $\tau_{\text{flow}} = 2R_c/\dot{L}_\infty$. Fig. 5*B* is obtained by running the model with an increasing number of cells to reproduce the aggregate's viscous flow. In this simulation, one cell is added every $\tau_{\text{flow}} = 6\tau_c$, cor-

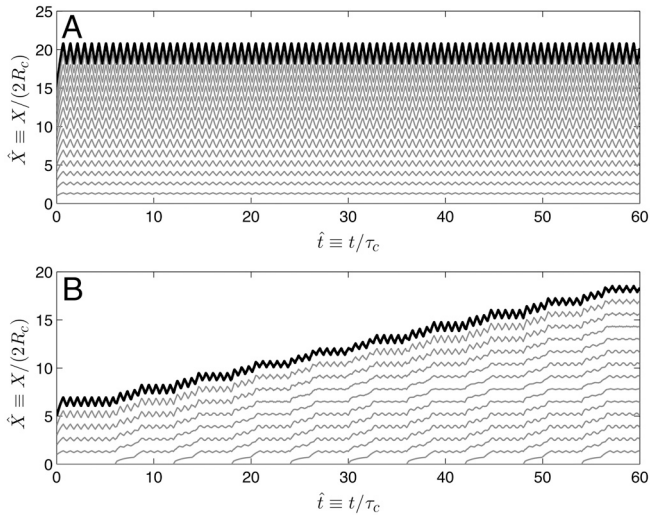


**Fig. 5.** (*A*) Aspiration curves predicted by the one-dimensional model for parameter values corresponding to a typical experiment ($\hat{F}_p = 0.5$, $N = 15$). The active cell response is characterized by $\hat{F}_m = 0.5$, $\epsilon_{\text{crit}} = 0.5$, $h = 100$, and $\hat{\tau}_s = 0.25$. The black curve corresponds to the position of the right-most cell edge, $X_N$, and the gray curves correspond to the other cell edges along the string. (*B*) Aspiration curves for the same parameter values but periodically increasing the number of cells to account for the viscous aggregate flow. The computation is started with $N = 5$ and one cell is added at the left end every six unit times, corresponding to the experimental observation that $\tau_{\text{flow}} \approx 6\tau_c$. The final number of cells is $N = 15$, as in the previous plot.

responding to the typical experimental ratio between these two timescales. Compared to Fig. 5*A*, Fig. 5*B* shows that, when some irregularity is added to the system, here by sequentially introducing cells into the pipette, the cell oscillations are not anymore in phase along the cell string. Thus, in plot Fig. 5*B* the amplitude of the oscillations does not increase with the number of cells in the string, and the oscillations remain much smaller than those in Fig. 5*A*. This result suggests that the amplitude of the small oscillations observed experimentally, of about 1 μm, is the oscillation amplitude of one single cell, whereas the less-frequent, larger oscillations must correspond to a momentaneous coupling between the oscillations of several cells, that add up their oscillation amplitudes to produce the larger shivering, as illustrated by Fig. 5*A*. We expect such momentaneous coupling to arise from the reorganization of cells inside the aggregate as they flow into the pipette, which has a characteristic time $\tau_{\text{flow}}$. Moreover, in a smaller aggregate the coupling of the contractions of a few cells in the aggregate body will have a more notorious effect, which could explain why the shivering is more pronounced in smaller aggregates. Indeed, the cell contractions due to aspiration-induced stretching extend to a region of size $R_p^3$ into the aggregate body outside the pipette. When the aggregate size is comparable to the pipette size, this region extends to most of the aggregate body. Thus, for smaller aggregates, cell contractions occur in most of the aggregate body and larger global oscillations are observed. In summary, the model rationalizes the two types of shivering oscillations that are observed experimentally: small-amplitude contractions with a shorter period $T_{\text{sc}} \approx 4\tau_s \approx 150$ s, corresponding to out-of-phase cell oscillations, and large-amplitude contractions with a longer period $T_{\text{lc}} \approx \tau_{\text{flow}} \approx 20$ min, corresponding to in-phase oscillations of several cells.

## Discussion

Force-induced synchronous cell oscillations are observed in tissue development, such as during gastrulation and dorsal closure in *Drosophila* (11, 15). In *Drosophila*, oscillations appear in the rather complex two-dimensional amnioserosa tissue. The aggregate shivering phenomenon described here is a simpler, one-dimensional laboratory model of these oscillatory active tissue response. From a physical perspective, aggregate shivering is at first sight reminiscent of avalanches in granular flow, where sudden large deformations take place due to stress relaxation. Unlike such avalanches, where grains collectively move in the direction of the forcing, the signature of aggregate shivering is a sudden contraction opposite to the applied pressure. This observation suggests that the origin of aggregate shivering is not stress relaxation but rather an active cellular response.

We explain the experimentally observed features of aggregate shivering by developing a physical model based on a delayed active contractile cell response. The nature of this active cell response was proposed by Solon et al. to describe cell oscillations in *Drosophila* (15): Each cell in the tissue responds with a delayed contraction when it is stretched beyond a deformation threshold. For aggregate aspiration, if the deformation imposed by the applied pressure is slightly above the threshold, cells will actively contract and decrease their deformation level to below the threshold. Then, after a time delay, the contractile force will stop, and cells will become again deformed beyond the threshold, thus establishing a cyclic response that results in shivering. In contrast, if the applied pressure is too low, no active contraction or shivering occurs. If the pressure is too high, cells are constantly contracted yielding a global reinforcement, but shivering does not occur either, because the cell contraction is not large enough to unstretch back the cells below the contractility threshold; this is why experimentally we only observe shivering for a narrow range of applied pressures (500–1,200 Pa). In combination with our physical model, the values of this pressure range suggest that the active contraction threshold corresponds to a cell stretching almost comparable to the cell's original size. Indeed, by fluorescently labeling the E-cadherins, we observe that cells in the aspirated tongue exhibit a deformed length of the order of twice its original diameter, as shown in Figs. 1*D* and 6*A* (Movie S1). From the observed pressure range, we also deduce that the magnitude of the cell contraction force is of the order of 0.1 μN. Active cell contractions, which according to our model should occur all along the aspirate tongue, are linked to actomyosin activity (11, 24). Accordingly, we find that fluorescently labeled phosphorilated Myosin II is expressed all along the aggregate tongue, as shown in Fig. 6 *B* and *C*. To verify the role of Myosin II in the shivering response, aggregates were treated with blebbistatin to inhibit Myosin II activity. The blebbistatin treatment suppresses aggregate shivering and accelerates the aspiration dynamics (Movie S3).

The model also suggests an explanation for the existence of the two characteristic timescales of shivering observed in the experiments: small oscillations with a shorter period (of about 50–300 s), and large oscillations with a longer period (of about 10–15 min). According to our model, the small oscillations correspond to out-of-phase individual cell contractility, and their period is approximately four times the time delay of the active

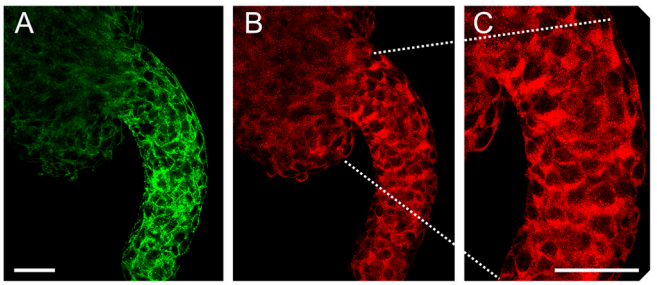


**Fig. 6.** Activation of Myosin II molecules in an aggregate aspirated for 2 h. The expression of E-cadherin and phosphorilated Myosin II molecules are marked using immunofluorescence techniques. (*A*) E-cadherin-GFP showing the contours of the cells. (*B*) Phosphorilated Myosin II. (*C*) Zoom of the tongue. (Scale bar: 50 μm for all images.)

contractions. This result implies a contraction response time of about 40 s, of the same order as the time delay observed by Solon et al. in amnioserosa cells in *Drosophila* (15). Contractions induced by laser activation, electrical stimulation, or chemical nanoperfusion in *Xenopus* embryos show comparable time delays (25). The longer period of oscillation corresponds to the coupling of oscillations between several cells arising from cell reorganization induced by the flow of cells from the aggregate body into the pipette, which has a characteristic timescale of about 10 min. In addition, our model suggests that the strength of the intercellular junctions is not a key parameter controlling the shivering processes. Indeed, we have performed experiments using cell lines with E-cadherin expression levels between 48% and 100% of that of our reference cell line, all of which show similar shivering behavior (Movie S4), although the range of pressures where shivering is observed varies slightly for different cell lines.

In an earlier study using the micropipette aspiration technique, Guevorkian et al. showed that a cellular aggregate increases its surface tension as a response to the applied aspiration pressure (18). The shivering behavior described here is another type of pressure-induced active cell reinforcement, in this case arising from an active contraction of cells as a response to stretching. Both effects can be globally regarded as manifestations of an active mechanical cell reinforcement in the presence of an external solicitation. The model presented here links the observed shivering contractions with the contractile response at the cell scale. Thus, our technique can next be applied to quantitatively characterize cell contractility in embryonic tissues in response to an applied external force.

## Materials and Methods

**Aggregate Preparation.** We used aggregates of murine sarcoma (S180) cell lines transfected to express different levels of E-cadherin molecules (26) (48%, 70%, and 100% of the reference cell line). Unless indicated otherwise, the results presented in this article correspond to the 70% expression level cell line, where the E-cadherins were tagged with GFP molecules. Cells were cultured under 5% $CO_2$ atmosphere in culture medium consisting of DMEM enriched with 10% calf serum. Confluent cells were detached using Trypsin/EDTA and resuspended in 5 mL of $CO_2$ equilibrated medium, at a concentration of 400,000 cells per mL. To form the aggregates, the suspension was transferred into 25-mL erlenmeyer flasks and placed in an orbital shaker at 75 rpm at 37 °C for 18–24 h, similar to Ryan et al. (27). The flasks were precoated with 2% dimethylchlorosilane in chloroform to prevent cell adhesion to the surface. Our experiments were performed on aggregates of diameters ranging from 150 to 300 μm. To inhibit Myosin II activity, the aggregates were incubated in 10 μM blebbistatin (Calbiochem) for 1 h before aspiration to insure penetration of the drug into the aggregate.

**Immunofluorescence Microscopy.** Aggregates were fixed in 4% paraformaldehyde in PBS + CaMg, rinsed, and incubated for several hours in PBTBG (PBS + 1%BSA + 0.15%glycine + 0.1%triton × 100) solution at 4 °C. They were subsequently incubated in PBTBG containing anti-E-cadherin (ECCD2, Takara) and antiphosphorylated Myosin II light chain (Ser19) (Cell Signaling) at 4 °C for 16 h, rinsed twice for 5 min, and then for 1 h in PBTBG. Aggregates were incubated in PBTBG containing anti-rat and anti-mouse IgG coupled to Alexa 488 and Alexa 594 (Molecular Probes), respectively, for 5 h, rinsed three times for 10 min, and mounted on coverslides in immumount medium (Shandon). Aggregates were viewed by a confocal Eclipse Ti inverted microscope (Nikon).

**Experimental Setup.** Experiments were performed in plastic Petri dishes. One milliliter of aggregate solution was diluted with few milliliters of fresh $CO_2$ equilibrated medium and placed in a dish. Micropipettes were prepared by pulling borosilicate capillaries (1 mm, 0.5 mm o.d./i.d.) using a laser-based puller (P-2000, Sutter Instrument Company). Afterward, the pipettes were sized by hand to a few tens of micrometers in diameter by using a quartz tile (Sutter Instrument Company). The tip of the pipettes were then smoothened by approaching to a heated filament (Narishige). With this technique, long straight tips between 60 and 80 μm in diameter were obtained. To introduce the pipette into the Petri dish, they were bent in a step-shape as shown in Fig. 1*A* by gently heating the pipette on a flame. Before the experiments, the pipettes were cleaned in a plasma cleaner and coated with 0.1 mg/mL polyethylene glycol-polylysine [PLL(20)-g[3.5]-PEG(2), Surface Solution] in Hepes solution (pH 7.3) for 1 h. The pipettes were then rinsed with Hepes and connected to a water reservoir attached to a vertical displacer (Velmex, UniSlide). By displacing the water reservoir with respect to the pipette tip, pressure differences with a precision of 10 Pa were obtained. Once the pipette was placed inside the chamber, the top of the chamber was covered with a layer of mineral oil (Sigma-Aldrich).

Aspirated aggregates were visualized on a Zeiss Axiovert 100 inverted microscope equipped with either a ×10 air objective N.A. = 0.3 or a ×20 air objective N.A. = 0.45, and recorded on a computer with a CCD camera (Cascade II, Photometrics) with a 5–10 s interval. The advancement of the aggregate inside the pipette and the contractions were quantified through the kymograph of the advancement of the projected aggregate inside the pipette using custom-made MatLab codes. The confocal imaging was performed on a Nikon TE2000 inverted microscope. All experiments were performed at 37 °C by means of a heated microscope stage.

**Numerical Model.** Our simplified one-dimensional model, consisting of a string of $N$ cells, is sketched in Fig. 4. $X_j$ denotes the position of the $j$th edge of the string, between the $j$th and the $(j+1)$th cell. Equilibrium at the $j$th edge at time $t$ of the viscoelastic forces exerted by the two neighboring cells requires

$$k_c(X_{j+1} - 2X_j + X_{j-1}) + \mu_c \frac{\partial}{\partial t}(X_{j+1} - 2X_j + X_{j-1}) = 0, \qquad [5]$$

where $t$ is the time. The first and second term on the left-hand side represent the elastic and the viscous cell responses, respectively. When an aspiration pressure is applied, Eq. **5** describes the evolution of the length of the aspiration tongue in time, which evolves exponentially during a characteristic time $\tau_c = \mu_c/k_c$ toward the equilibrium elastic deformation corresponding to the applied pressure. In addition, we consider the active cell contractile forces and write

$$k_c(X_{j+1} - 2X_j + X_{j-1}) + \mu_c \frac{\partial}{\partial t}(X_{j+1} - 2X_j + X_{j-1}) + F_m[f_{j+1}(t-\tau_s) - f_j(t-\tau_s)] = 0, \qquad [6]$$

where $f_j(t-\tau_s)$ determines the instantaneous contractile force exerted by the $j$th cell. Whereas in our analytical description we represented the contractile response by a step function, for the numerical solution we use a continuous representation given by a Hill function, as previously done by Solon et al. (15). Thus, the contractile force is given by

$$f_j(t-\tau_s) = \frac{\epsilon_j(t-\tau_s)^h}{\epsilon_j(t-\tau_s)^h + \epsilon_{\text{crit}}^h} = \frac{[X_j(t-\tau_s) - X_{j-1}(t-\tau_s) - 2R_c]^h}{[X_j(t-\tau_s) - X_{j-1}(t-\tau_s) - 2R_c]^h + (2R_c\epsilon_{\text{crit}})^h}, \qquad [7]$$

where $\epsilon_j = (X_j - X_{j-1})/2R_c - 1$ is the strain of the $j$th cell, and $h$ is the Hill coefficient that controls the slope of the function, with a larger $h$ corresponding to a steeper variation from 0 to $F_m$ near $\epsilon = \epsilon_{\text{crit}}$. We take $h = 100$ in order to have a steep variation that resembles the step function. We nondimensionalize these governing equations by using $2R_c$ and $\tau_c = \mu_c/k_c$ as length and timescales, respectively. The resulting nondimensional variables are denoted by $\hat{X} \equiv X/(2R_c)$ and $\hat{t} \equiv t/\tau_c$. The nondimensional form of Eq. **6** is

$$(\hat{X}_{j+1} - 2\hat{X}_j + \hat{X}_{j-1}) + \left(\frac{\partial \hat{X}_{j+1}}{\partial \hat{t}} - 2\frac{\partial \hat{X}_j}{\partial \hat{t}} + \frac{\partial \hat{X}_{j-1}}{\partial \hat{t}}\right) + \hat{F}_m[f_{j+1}(\hat{t}-\hat{\tau}_s) - f_j(\hat{t}-\hat{\tau}_s)] = 0, \qquad [8]$$

where $\hat{F}_m \equiv F_m/(2k_cR_c)$ and $\hat{\tau}_s \equiv \tau_s/\tau_c$. Initially, cells are assumed to be at their equilibrium position, $\hat{X}_j(t=0) = j$. The left boundary is fixed, $\hat{X}_0 = 0$. On the right boundary, we prescribe the balance of the viscoelastic response and contractile force of the last cell with the applied aspiration force, $\hat{F}_p \equiv F_p/(2k_cR_c)$. The system of Eq. **8** can be solved numerically to obtain the position of the cell edges, $\hat{X}_j$ for $0 \le \hat{X}_j \le N$, where $N$ is the number of cells in the string. The nondimensional parameters of the problem are thus $\hat{F}_p$, the nondimensional aspiration force; $\hat{F}_m$, the nondimensional maximum active contractile force; $\epsilon_{\text{crit}}$, the critical strain for cell contraction; $\hat{\tau}_s$, the nondimensional delay for cell contraction; and $h$, the Hill coefficient. As discussed above, the model can be run using a fixed number of cells $N$ or with a number that increases by one unit every $\tau_{\text{flow}}$.

**ACKNOWLEDGMENTS.** The authors thank P. Bassereau's group for providing access to their confocal microscope. The authors greatly acknowledge the Nikon Imaging Center at Institut Curie-Centre National de la Recherche Scientifique (CNRS) and V. Fraisier and L. Sengmanivong for their help with imaging. The group belongs to the CNRS consortium CellTiss. F.B.-W. and S.D. thank the Curie Programme Incitatif et Coopératif for funding. D.G.-R. is supported by the Fondation Pierre-Gilles de Gennes. C.C. is supported by the CNRS and the Institut Curie.

1. Desprat N, Supatto W, Pouille P-A, Beaurepaire E, Farge E (2008) Tissue deformation modulates twist expression to determine anterior midgut differentiation in Drosophila embryos. *Dev Cell* 15:470–477.
2. Pouille P-A, Ahmadi P, Brunet A-C, Farge E (2009) Mechanical signals trigger myosin II redistribution and mesoderm invagination in drosophila embryos. *Sci Signal* 2:ra16.
3. Engler AJ, Sen S, Sweeney HL, Discher DE (2006) Matrix elasticity directs stem cell lineage specification. *Cell* 126:677–689.
4. Schwartz MA, DeSimone DW (2008) Cell adhesion receptors in mechanotransduction. *Curr Opin Cell Biol* 20:551–556.
5. Papusheva E, Heisenberg C-P (2010) Spatial organization of adhesion: Force-dependent regulation and function in tissue morphogenesis. *EMBO J* 29:2753–2768.
6. Wang N, Butler JP, Ingber DE (1993) Mechanotransduction across the cell surface and through the cytoskeleton. *Science* 260:1124–1127.
7. Riveline D, et al. (2001) Focal contacts as mechanosensors: Externally applied local mechanical force induces growth of focal contacts by an mdia1-dependent and rock-independent mechanism. *J Cell Biol* 153:1175–1186.
8. Le Duc Q, et al. (2010) Vinculin potentiates E-cadherin mechanosensing and is recruited to actin-anchored sites within adherens junctions in a myosin II-dependent manner. *J Cell Biol* 189:1107–1115.
9. Rauzi M, Verant P, Lecuit T, Lenne P-F (2008) Nature and anisotropy of cortical forces orienting drosophila tissue morphogenesis. *Nat Cell Biol* 10:1401–1410.
10. Landsberg KP, et al. (2009) Increased cell bond tension governs cell sorting at the drosophila anteroposterior compartment boundary. *Curr Biol* 19:1950–1955.
11. Martin AC, Kaschube M, Wieschaus EF (2009) Pulsed contractions of an actin-myosin network drive apical constriction. *Nature* 457:495–499.
12. Sawyer JM, et al. (2010) Apical constriction: A cell shape change that can drive morphogenesis. *Dev Biol* 341:5–19.
13. Nakajima Y, Burke RD (1996) The initial phase of gastrulation in sea urchins is accompanied by the formation of bottle cells. *Dev Biol* 179:436–446.
14. Haigo SL, Hildebrand JD, Harland RM, Wallingford JB (2003) Shroom induces apical constriction and is required for hingepoint formation during neural tube closure. *Curr Biol* 13:2125–2137.
15. Solon J, Kaya-Copur A, Colombelli J, Brunner D (2009) Pulsed forces timed by a ratchet-like mechanism drive directed tissue movement during dorsal closure. *Cell* 137:1331–1342.
16. Foty RA, Forgacs G, Pfleger CM, Steinberg MS (1994) Liquid properties of embryonic tissues: Measurement of interfacial tensions. *Phys Rev Lett* 72:2298–2301.
17. Mgharbel A, Delanoë-Ayari H, Rieu J-P (2009) Measuring accurately liquid and tissue surface tension with a compression plate tensiometer. *HFSP J* 3:213–221.
18. Guevorkian K, Colbert M-J, Durth M, Dufour S, Brochard-Wyart F (2010) Aspiration of biological viscoelastic drops. *Phys Rev Lett* 104:218101.
19. Kalantarian A, et al. (2009) Axisymmetric drop shape analysis for estimating the surface tension of cell aggregates by centrifugation. *Biophys J* 96:1606–1616.
20. Foty RA, Steinberg MS (2005) The differential adhesion hypothesis: A direct evaluation. *Dev Biol* 278:255–263.
21. Krieg M, et al. (2008) Tensile forces govern germ-layer organization in zebrafish. *Nat Cell Biol* 10:429–436.
22. Manning ML, Foty RA, Steinberg MS, Schoetz E-M (2010) Coaction of intercellular adhesion and cortical tension specifies tissue surface tension. *Proc Natl Acad Sci USA* 107:12517–12522.
23. Micoulet A, Spatz JP, Ott A (2005) Mechanical response analysis and power generation by single-cell stretching. *Chemphyschem* 6:663–670.
24. Kruse K, Riveline D (2011) Spontaneous mechanical oscillations: Implications for developing organisms. *Curr Top Dev Biol* 95:67–91.
25. Joshi SD, von Dassow M, Davidson LA (2010) Experimental control of excitable embryonic tissues: Three stimuli induce rapid epithelial contraction. *Exp Cell Res* 316:103–114.
26. Chu YS, et al. (2004) Force measurements in E-cadherin mediated cell doublets reveal rapid adhesion strengthened by actin cytoskeleton remodeling through rac and cdc42. *J Cell Biol* 167:1183–1194.
27. Ryan PL, Foty RA, Kohn J, Steinberg MS (2001) Tissue spreading on implantable substrates is a competitive outcome of cell-cell vs. cell-substratum adhesivity. *Proc Natl Acad Sci USA* 98:4323–4327.